

Quark and gluon momentum fractions in the pion from $N_f = 2 + 1 + 1$ lattice QCD

Constantia Alexandrou,^{1,2} Simone Bacchio,² Georg Bergner,³ Jacob Finkenrath,² Andrew Gasbarro,⁴
Kyriakos Hadjiyiannakou,^{1,2} Karl Jansen,⁵ Bartosz Kostrzewa,⁶ Konstantin Ottnad,⁷ Marcus
Petschlies,^{8,9} Ferenc Pittler,² Fernanda Steffens,^{8,9} Carsten Urbach,^{8,9} and Urs Wenger^{4,10}

(Extended Twisted Mass Collaboration)

¹*Department of Physics, University of Cyprus, Nicosia, Cyprus*

²*Computation-based Science and Technology Research Center, The Cyprus Institute, Nicosia, Cyprus*

³*Institute of Theoretical Physics, Friedrich Schiller University Jena, Germany*

⁴*Albert Einstein Center, Institute for Theoretical Physics, University of Bern, Switzerland*

⁵*NIC, DESY Zeuthen, Germany*

⁶*High Performance Computing and Analytics Lab,
Rheinische Friedrich-Wilhelms-Universität Bonn, Germany*

⁷*PRISMA+ Cluster of Excellence and Institut für Kernphysik,
Johannes Gutenberg-Universität Mainz, Germany*

⁸*Helmholtz-Institut für Strahlen- und Kernphysik, University of Bonn, Germany*

⁹*Bethe Center for Theoretical Physics, University of Bonn, Germany*

¹⁰*Department of Theoretical Physics, CERN, Geneva, Switzerland*

(Dated: February 9, 2022)

We perform the first full decomposition of the pion momentum into its gluon and quark contributions. We employ an ensemble generated by the Extended Twisted Mass Collaboration with $N_f = 2 + 1 + 1$ Wilson twisted mass clover fermions at maximal twist tuned to reproduce the physical pion mass. We present our results in the $\overline{\text{MS}}$ scheme at 2 GeV. We find $\langle x \rangle_{u+d} = 0.601(28)$, $\langle x \rangle_s = 0.059(13)$, $\langle x \rangle_c = 0.019(05)$, and $\langle x \rangle_g = 0.52(11)$ for the separate contributions, respectively, whose sum saturates the momentum sum rule.

Introduction.— Quantum Chromodynamics (QCD) manifests itself in the form of a plethora of states – so called hadrons, formed by quarks and gluons. Pions are particularly interesting hadrons: they are the lightest and simplest of the QCD bound states composed out of quark and antiquark. At the same time pions are also pseudo-Goldstone bosons, with the spontaneous breaking of chiral symmetry playing a fundamental role in the emergence of their mass. Yet, in contrast to the nucleon (proton and neutron), a first principles computation of the pion structure, and in particular how quarks and gluons contribute to its mass and momentum decomposition is still lacking. The importance of this topic is well represented in the Electron Ion Collider (EIC) yellow report [1]: eight main science questions concerning pions (and kaons) are prominently put forward. Let us highlight two of these questions here: “What are the quark and gluon energy contributions to the pion mass?”, and “Is the pion full or empty of gluons as viewed at large Q^2 ?” The results presented in this letter on the momentum decomposition of the pion using lattice QCD simulations address both questions.

As mentioned before, there is a wealth of studies on the nucleon momentum decomposition available in the literature using phenomenological analyses of experimental data [2–5], and, more recently, from precise simulations of lattice QCD at the physical point [6, 7]. The reason for the pion being much less well investigated is that proton

and neutron structure is experimentally well accessible, while the pion is significantly more challenging because there is no pion target available. For that reason, only recently the first Monte Carlo global QCD analysis for pion PDFs has been presented in Ref. [8], which includes leading neutron electroproduction (LNE) data from HERA and Drell-Yan data from CERN and Fermilab. One of their interesting findings is that the decomposition of the pion momentum, $\langle x \rangle_\pi$, into its valence, $\langle x \rangle_v$, sea, $\langle x \rangle_s$, and gluon, $\langle x \rangle_g$ components depends strongly on which data set is included in the analysis. In particular, the inclusion of LNE data, which induces a model dependence in the extraction of the pion PDFs, has a significant effect on the average momentum carried by gluons and sea quarks in the pion. Precise lattice QCD data for both quark and gluon momentum fractions has, thus, the potential to add new model independent constraints on the extraction of pion PDFs from experimental data. Finally, new data coming from planned EIC experiments, as well as from COMPASS++/Amber [9] will help to clarify the quark and gluon dynamics within the pion.

On the theory side one has to resort to models [10, 11] or to nonperturbative methods as provided by lattice QCD. Also from the lattice side, there is surprisingly little known for the pion. Most of the computations available so far [12–19] neglect potentially important contributions, the so-called quark disconnected contributions. While we were finalising the present work a first com-

putation including disconnected contributions was put forward [20]. Also for the gluon contributions there exists only a single computation and only in the quenched approximation [21]. Thus, systematics are certainly not sufficiently controlled. More recently, there are studies using quasi- [22–25] and pseudo-distributions [26, 27] as well as so-called good lattice cross sections [28–30] approaches to compute the x dependence of the pion PDFs directly on the lattice. These studies, however, are restricted to connected contributions only.

In this letter we present the first calculation of the quark and gluon momentum fractions in the pion based on lattice QCD simulations with $N_f = 2 + 1 + 1$ dynamical quark flavours including all required contributions. The computation is performed using one ensemble with physical values of all four quark mass parameters. This allows us to check the momentum sum rule, i.e. whether all four quark and the gluon fractions sum up to one. This result can pave the way towards a global QCD analysis including experimental data as well as lattice QCD results of the pion, which will help to sort out the discrepancy found between different experimental data sets.

Lattice Computation.— Our computation is based on an ensemble [31] generated by the Extended Twisted Mass Collaboration (ETMC) using $N_f = 2 + 1 + 1$ dynamical Wilson twisted mass clover fermions at maximal twist [32, 33] and Iwasaki gauge action [34]. With this discretisation, lattice artefacts are of $O(a^2)$ only [35]. The lattice volume is $L^3 \times T = 64^3 \times 128$ and the lattice spacing $a = 0.08029(41)$ fm. For strange and charm quarks we use a mixed action approach following Ref. [36], and all quark mass parameters are tuned to assume approximately physical values [31, 37]. We give further details on quark mass tuning in the appendix. For all estimates we used 745 well-separated gauge configurations.

The relevant elements of the traceless Euclidean energy-momentum tensor (EMT) for quark flavour q with the symmetrised covariant derivative $\overleftrightarrow{D}_\mu$ read

$$\bar{T}_{\mu\nu}^q = -\frac{(i)^{\kappa_{\mu\nu}}}{4} \bar{q} \left(\gamma_\mu \overleftrightarrow{D}_\nu + \gamma_\nu \overleftrightarrow{D}_\mu - \delta_{\mu\nu} \frac{1}{2} \gamma_\rho \overleftrightarrow{D}_\rho \right) q, \quad (1)$$

with $\kappa_{\mu\nu} = \delta_{\mu,4} \delta_{\nu,4}$. Analogously for the gluon

$$\bar{T}_{\mu\nu}^g = (i)^{\kappa_{\mu\nu}} \left(F_{\mu\rho} F_{\nu\rho} + F_{\nu\rho} F_{\mu\rho} - \delta_{\mu\nu} \frac{1}{2} F_{\rho\sigma} F_{\rho\sigma} \right). \quad (2)$$

For $X = u, d, s, c, g$, one then obtains $\langle x \rangle^X$ from

$$\langle \pi(\mathbf{p}) | \bar{T}_{\mu\nu}^X | \pi(\mathbf{p}) \rangle = 2 \langle x \rangle^X \left(p_\mu p_\nu - \delta_{\mu\nu} \frac{p^2}{4} \right) \quad (3)$$

with on-shell momentum $p = (E_\pi = \sqrt{m_\pi^2 + \mathbf{p}^2}, \mathbf{p})$. We extract these matrix elements from ratios of Euclidean

three- and two-point functions

$$R_{\mu\nu}^X(t, t_f, t_i; \mathbf{p}) = \frac{\langle \pi(t_f, \mathbf{p}) | \bar{T}_{\mu\nu}^X(t) | \pi(t_i, \mathbf{p}) \rangle}{\langle \pi(t_f, \mathbf{p}) | \pi(t_i, \mathbf{p}) \rangle} \quad (4)$$

which are related to the matrix element

$$R_{\mu\nu}^X(t, t_f, t_i; \mathbf{p}) \rightarrow \frac{1}{2E_\pi} \frac{\langle \pi(\mathbf{p}) | \bar{T}_{\mu\nu}^X | \pi(\mathbf{p}) \rangle}{1 + \exp(-E_\pi(T - 2(t_f - t_i)))} \quad (5)$$

for $t_f - t, t - t_i$ (and thus $t_f - t_i$) large enough such that excited state contributions have decayed sufficiently. At the same time $T \gtrsim 2(t_f - t_i)$ should be maintained, otherwise finite size effects become sizable via excited states contaminations. R depends on $t_f - t_i$ and $t - t_i$ only, and in the following we set $t_i = 0$.

According to Eq. (3), $\langle x \rangle$ can be extracted with zero pion momentum from tensor elements with $\mu = \nu$, whereas for $\mu \neq \nu$ nonzero momentum is required. In general, one might expect the signal to be noisier with nonzero momentum, and this is indeed the case for the connected-only contribution. However, due to the fact that for $\mu = \nu$ the signal requires the subtraction of the trace of the EMT, the quark disconnected and gluon contributions are better determined from the off-diagonal elements of the EMT, see also Ref. [7]. Therefore, we determine the connected-only light contribution to $\langle x \rangle$ from \bar{T}_{44} at zero pion momentum $\mathbf{p} = 0$, and all the other contributions from \bar{T}_{4k} with smallest nonzero momentum $|\mathbf{p}| = 2\pi/L$, averaged over all six spatial directions. Further justification for using (off-) diagonal tensor elements for (dis-)connected diagrams is given in the appendix.

For the light-quark connected part both two- and three-point functions are constructed using stochastic timeslice sources with spin-color-site components independently and identically distributed, according to $(\mathbb{Z}_2 + i\mathbb{Z}_2)/\sqrt{2}$, with random \mathbb{Z}_2 noise and eight stochastic samples per gauge field configuration. For the quark-disconnected part of any quark flavour, as well as the gluon operator part, we employ point-to-all propagators with 200 randomly distributed source points per configuration and full spin-color dilution to estimate the pion two-point function. The light-quark loop diagrams with covariant derivative insertion are determined based on the combination of low-mode deflation [38] of the Dirac operator with 200 eigenmodes, and hierarchical probing [39] with one stochastic volume source decomposed to coloring distance of eight lattice sites in each spatial direction. Spin-color dilution is also employed. The strange quark is treated with the same hierarchical probing setup, but without deflation. Analogously, for the charm-quark loops we use 12 spin-color diluted volume sources with coloring distance 4 [7]. The gluon field strength tensor in the gluon operator matrix element is computed with the clover field definition, see e.g. [40]. We apply ten levels of stout smearing [41] to the gauge links in order to sufficiently reduce ultraviolet fluctuations, see Ref. [6, 7].

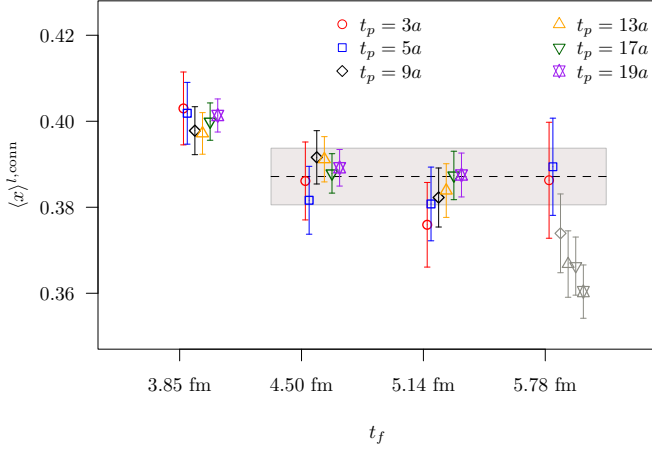


FIG. 1. Fit results for the bare light connected $\langle x \rangle^{l, \text{conn}}$ as a function of t_f for different fit range values t_p . Greyed out points have a $\chi^2/\text{dof} > 1.3$. Grey band and dashed line represent the result and total error obtained via a weighted averaging procedure.

Errors are computed using the bootstrap method with fully correlated fits. Since lattice artefacts are of $\mathcal{O}(a^2)$ with our discretisation, we expect discretisation errors generically of the size $a^2 \Lambda_{\text{QCD}}^2$. For the value of the lattice spacing a used here this amounts to $\sim 2.6\%$ with unknown coefficient.

Renormalisation.— The quark flavour-nonsinglet combinations renormalise with Z_{qq} as

$$\begin{aligned} \langle x \rangle_{u-d}^{\text{R}} &= Z_{qq}(\langle x \rangle_u - \langle x \rangle_d), \\ \langle x \rangle_{u+d-2s}^{\text{R}} &= Z_{qq}(\langle x \rangle_u + \langle x \rangle_d - 2\langle x \rangle_s), \\ \langle x \rangle_{u+d+s-3c}^{\text{R}} &= Z_{qq}(\langle x \rangle_u + \langle x \rangle_d + \langle x \rangle_s - 3\langle x \rangle_c). \end{aligned} \quad (6)$$

For the pion, $\langle x \rangle_{u-d}^{\text{R}} = 0$ in the isospin symmetric case, as simulated here. The quark-singlet and gluon components mix under renormalisation according to

$$\begin{pmatrix} \langle x \rangle_f^{\text{R}} \\ \langle x \rangle_g^{\text{R}} \end{pmatrix} = \begin{pmatrix} Z_{qq}^s & Z_{qg} \\ Z_{gq} & Z_{gg} \end{pmatrix} \begin{pmatrix} \langle x \rangle_f \\ \langle x \rangle_g \end{pmatrix} \quad (7)$$

with Z_{qq}^s the quark-singlet renormalisation constant. Defining $\delta Z_{qq} = Z_{qq}^s - Z_{qq}$, one can solve the set of Eqs. (7) for each single flavour and gluon component:

$$\begin{aligned} \langle x \rangle_f^{\text{R}} &= Z_{qq} \langle x \rangle_f + \frac{\delta Z_{qq}}{N_f} \sum_{f'} \langle x \rangle_{f'} + \frac{Z_{qg}}{N_f} \langle x \rangle_g, \\ \langle x \rangle_g^{\text{R}} &= Z_{gg} \langle x \rangle_g + Z_{gq} \sum_{f'} \langle x \rangle_{f'}. \end{aligned} \quad (8)$$

Due to lattice artefacts, renormalisation factors are different for $\bar{T}_{\mu\nu}$ with $\mu = \nu$ and $\mu \neq \nu$. The diagonal elements of the renormalisation matrix have been determined nonperturbatively and the off-diagonal elements perturbatively in Ref. [7], see also the appendix. Since

these mixing coefficients have been determined using one-loop perturbation theory, we do not have an error estimate available. In order to account for the uncertainty, we perform the computation once including the mixing, and once excluding it, and take the spread as error estimate.

Results.— We compute $R^X(t)$ in Eq. (4) for various values of t_f . Solving Eq. (3) for $\langle x \rangle$ and inserting Eq. (5), we then extract $\langle x \rangle^X(t)$, where X stands for l, conn (with $l \equiv u + d$), l, disc , s , c , and g . For large enough t_f we expect $\langle x \rangle(t)$ to show a plateau for $t - t_f/2$ around 0. Thus, we fit a constant symmetrically around $t - t_f/2 = 0$ with fit range denoted as t_p to our bare data for $\langle x \rangle(t)$ (for plots of this bare data see the appendix). In Fig. 1 we show the result of such constant fits to the light connected contribution as a function of the source-sink separation t_f for different values of t_p . Between $t_f = 4.5$ fm and $t_f = 5.14$ fm we see agreement for all values of t_p . For $t_f = 5.78$ fm the results for the smallest three t_p values still agree with the previous ones. However, for the larger t_p values we start to see finite size effects due to $T/2 < t_f$, also visible in the bad χ^2/dof values.

In Fig. 2 we again show the fit results as a function of t_f for different t_p values, but here for the light disconnected and the strange, charm and gluon contributions. For the quark disconnected contributions we loose the signal for $t_f > 2.25$ fm. However, for all three cases we observe agreement between all results for $1.61 \text{ fm} \leq t_f \leq 2.25 \text{ fm}$, confirming ground state dominance. Thus, we are confident that the final result can be determined in this region of t_f values.

We arrive at the final result by assigning a weight $w = \exp(-\frac{1}{2}[\chi^2 - 2 \text{dof}])$ to every fit with given χ^2 value and degrees of freedom (dof). Then we take the weighted average (see also [42]) over all constant fits in the aforementioned regions of t_f values. The *combined statistical and systematic* error is computed by repeating this procedure on all bootstrap samples with weights corresponding to the fits on the samples. Alternatively, we have also performed fits which take explicitly into account excited state contaminations again for various t_f and t_p values leading to consistent results, but with a different distribution of statistical and systematic errors.

Using the so extracted bare values for $\langle x \rangle^X$ (see the appendix), we are now in the position to compute the renormalised flavour nonsinglet and singlet contributions to $\langle x \rangle$. We obtain for the nonsinglet ones from Eq. (6)

$$\langle x \rangle_{u+d-2s}^{\text{R}} = 0.48(1), \quad \langle x \rangle_{u+d+s-3c}^{\text{R}} = 0.60(3), \quad (9)$$

where we recall that $\langle x \rangle_{u-d} = 0$ due to isospin symmetry in the light-quark sector. For the singlet contributions we find, using Eqs. (7) and (8),

$$\sum_f \langle x \rangle_f^{\text{R}} = 0.68(5)_{(-)}, \quad \langle x \rangle_g^{\text{R}} = 0.52(11)^{(+2)}. \quad (10)$$

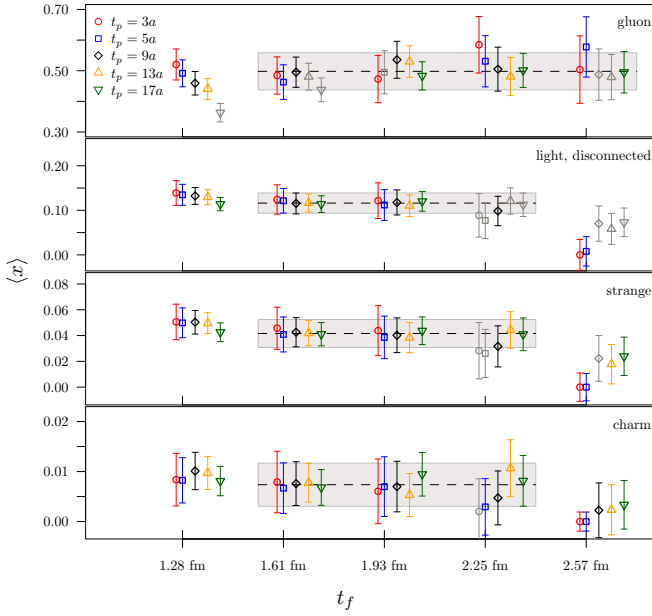


FIG. 2. Fit results for the bare quark disconnected and the gluon $\langle x \rangle$ as a function of t_f for different fit range values t_p . Greyed out points have a $\chi^2/\text{dof} > 1.3$. Grey band and dashed line represent the result and total error obtained via a weighted averaging procedure.

The first error represents the combined statistical and fit range uncertainty, the second error comes from the mixing under renormalisation. The sum of all contributions amounts to $\langle x \rangle_{\text{total}}^R = 1.20(13)(-3)$, compatible with the expected value of 1 within two sigma. This is an important result because, in contrast to phenomenological analyses where the saturation of the momentum sum rule is imposed, in our work such saturation is a result of the computation. In Fig. 3 we compare to the recent phenomenological results [43] from Ref. [44] and Ref. [45]. Our work agrees within errors with these state-of-art phenomenological results.

In Table I we compile all the contributions again and compare to the literature. The only other lattice result was presented in Ref. [20], where $N_f = 2 + 1$ flavour QCD was used and results have been extrapolated to the continuum and the physical point. However, the gluon contribution has not been computed and, thus, the mixing could not be taken into account. Therefore, the comparison of the quark singlet contributions is of limited meaningfulness. The nonsinglet contribution $\langle x \rangle_{u+d-2s}^R$ is better suited for a comparison. While currently there is a discrepancy between the results, we notice that a full comparison should be attempted only after the inclusion of all unaccounted systematics.

Finally, the results from the momentum sum rule decomposition can be used to determine how quarks and gluons contribute to the pion mass. In principle, mass can be decomposed in QCD in different ways [46–51]. Choos-

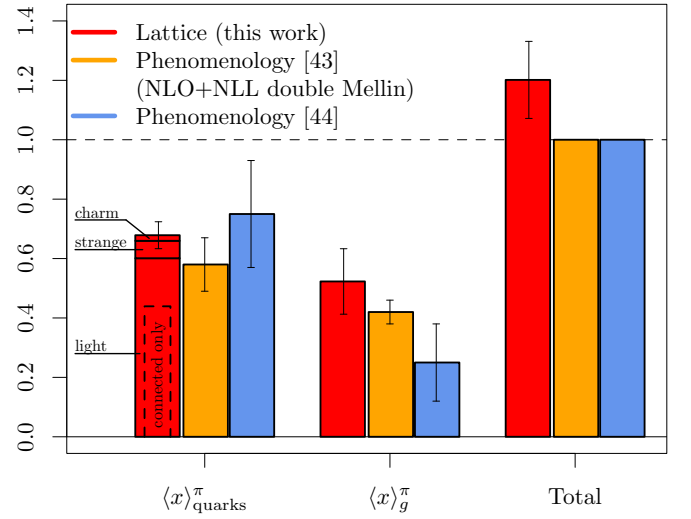


FIG. 3. Comparison to Ref. [44] and Ref. [45] at 2 GeV in the $\overline{\text{MS}}$ scheme. In the two phenomenological computations the momentum sum rule is imposed.

ing the sum rule of Ref. [51], $M_{\pi,q} = (3M_\pi/4)\langle x \rangle_{\text{quarks}}^R$ and $M_{\pi,g} = (3M_\pi/4)\langle x \rangle_g^R$, which amounts to 70(5) MeV and 55(12) MeV at 2 GeV in the $\overline{\text{MS}}$ scheme, respectively. Note that the gluon contribution is the same in Ji’s original mass decomposition [46, 47]. The remaining contribution is split among a trace anomaly term and a term proportional to the quark mass.

	this work	[20]	[44]	[45]
$\langle x \rangle_l^R$	0.601(28)($_{-21}$)	–	–	–
$\langle x \rangle_s^R$	0.059(13)($_{-10}$)	–	–	–
$\langle x \rangle_c^R$	0.019(05)($_{-10}$)	–	–	–
$\langle x \rangle_g^R$	0.52(11)($^{+02}$)	–	0.42(4)	0.25(13)
$\sum_f \langle x \rangle_f^R$	0.68(05)($_{-03}$)	0.220(207)	0.58(9)	0.75(18)
$\langle x \rangle_{u+d-2s}^R$	0.48(01)	0.344(28)	–	–
$\langle x \rangle_{u+d+s-3c}^R$	0.60(03)	–	–	–

TABLE I. Compilation of results and comparison to literature. All values are at 2 GeV in the $\overline{\text{MS}}$ scheme.

Summary and Outlook. — In this letter we have presented results for the complete flavour decomposition of the average momentum of quarks and gluons in the pion for the first time. The computation in $N_f = 2+1+1$ lattice QCD are performed directly with physical values of the quark mass parameters making an extrapolation to the physical point superfluous and, thus, avoiding any systematic uncertainty from such an extrapolation. However, we work at a single value of the lattice spacing only, which does not allow us to take the continuum limit. Therefore, we have to expect lattice artefacts of $\mathcal{O}(a^2)$ which we cannot account for rigorously. The renormalisation constants have been computed nonperturbatively, while the mixing coefficients were computed in perturbation theory.

We find the momentum sum rule to be fulfilled within two sigma errors, see Fig. 3. When comparing to phenomenological determinations from Refs. [44, 45] we find reasonable agreement within relatively large uncertainties. Comparing to the only other lattice QCD computation [20] including quark disconnected contributions, but not the mixing and the gluon contribution, we observe a deviation well outside uncertainties.

Future plans include determining $\langle x \rangle$ in the pion for two more lattice spacing values directly at the physical point. Preliminary results for the flavour non-singlet components at a finer lattice spacing show agreement within errors. Moreover, work is in progress to determine the mixing coefficients nonperturbatively. This work opens the possibility to combine lattice QCD results and experimental data in a global phenomenological analysis.

Acknowledgements.— The authors thank M. Constantinou for very helpful discussions and gratefully acknowledge the Gauss Centre for Supercomputing e.V. (www.gauss-centre.eu) for funding this project by providing computing time on the GCS Supercomputer JUQUEEN [52] and the John von Neumann Institute for Computing (NIC) for computing time provided on the supercomputers JURECA [53] and JUWELS [54] at Jülich Supercomputing Centre (JSC). We further acknowledge computing time granted on Piz Daint at Centro Svizzero di Calcolo Scientifico (CSCS) via the project with ids s849, s702 and s954. This work is supported in part by the Deutsche Forschungsgemeinschaft (DFG, German Research Foundation) and the NSFC through the funds provided to the Sino-German Collaborative Research Center CRC 110 “Symmetries and the Emergence of Structure in QCD” (DFG Project-ID 196253076 - TRR 110, NSFC Grant No. 12070131001), the Swiss National Science Foundation (SNSF) through grant No. 200021_175761 and the Marie Skłodowska-Curie European Joint Doctorate STIMULATE funded by the European Union’s Horizon 2020 research & innovation program under Grant agreement No. 765048. FP acknowledges financial support from the Cyprus Research and Innovation Foundation under project “NextQCD”, contract no. EXCELLENCE/0918/0129. The open source software packages tmLQCD [55–57], Lemon [58], QUDA [59–61] and R [62, 63] have been used.

[1] R. Abdul Khalek *et al.*, “Science Requirements and Detector Concepts for the Electron-Ion Collider: EIC Yellow Report,” (2021), [arXiv:2103.05419 \[physics.ins-det\]](#).
[2] Richard D. Ball *et al.* (NNPDF), “Parton distributions from high-precision collider data,” *Eur. Phys. J. C* **77**, 663 (2017), [arXiv:1706.00428 \[hep-ph\]](#).
[3] Sayipjamal Dulat, Tie-Jiun Hou, Jun Gao, Marco Guzzi, Joey Huston, Pavel Nadolsky, Jon Pumplin, Carl Schmidt, Daniel Stump, and C. P. Yuan, “New par-

ton distribution functions from a global analysis of quantum chromodynamics,” *Phys. Rev. D* **93**, 033006 (2016), [arXiv:1506.07443 \[hep-ph\]](#).
[4] S. Alekhin, J. Blümlein, S. Moch, and R. Placakyte, “Parton distribution functions, α_s , and heavy-quark masses for LHC Run II,” *Phys. Rev. D* **96**, 014011 (2017), [arXiv:1701.05838 \[hep-ph\]](#).
[5] Eric Moffat, Wally Melnitchouk, T. C. Rogers, and Nobuo Sato (Jefferson Lab Angular Momentum (JAM)), “Simultaneous Monte Carlo analysis of parton densities and fragmentation functions,” *Phys. Rev. D* **104**, 016015 (2021), [arXiv:2101.04664 \[hep-ph\]](#).
[6] C. Alexandrou, M. Constantinou, K. Hadjiyiannakou, K. Jansen, C. Kallidonis, G. Koutsou, A. Vaquero Avilés-Casco, and C. Wiese, “Nucleon Spin and Momentum Decomposition Using Lattice QCD Simulations,” *Phys. Rev. Lett.* **119**, 142002 (2017), [arXiv:1706.02973 \[hep-lat\]](#).
[7] C. Alexandrou, S. Bacchio, M. Constantinou, J. Finkenrath, K. Hadjiyiannakou, K. Jansen, G. Koutsou, H. Panagopoulos, and G. Spanoudes, “Complete flavor decomposition of the spin and momentum fraction of the proton using lattice QCD simulations at physical pion mass,” *Phys. Rev. D* **101**, 094513 (2020), [arXiv:2003.08486 \[hep-lat\]](#).
[8] P. C. Barry, N. Sato, W. Melnitchouk, and Chueng-Ryong Ji, “First Monte Carlo Global QCD Analysis of Pion Parton Distributions,” *Phys. Rev. Lett.* **121**, 152001 (2018), [arXiv:1804.01965 \[hep-ph\]](#).
[9] B. Adams *et al.*, “Letter of Intent: A New QCD facility at the M2 beam line of the CERN SPS (COMPASS++/AMBER),” (2018), [arXiv:1808.00848 \[hep-ex\]](#).
[10] Minghui Ding, Khépani Raya, Daniele Binosi, Lei Chang, Craig D Roberts, and Sebastian M. Schmidt, “Symmetry, symmetry breaking, and pion parton distributions,” *Phys. Rev. D* **101**, 054014 (2020), [arXiv:1905.05208 \[nucl-th\]](#).
[11] Adam Freese, Ian C. Cloët, and Peter C. Tandy, “Gluon PDF from Quark dressing in the Nucleon and Pion,” (2021), [arXiv:2103.05839 \[hep-ph\]](#).
[12] G. Martinelli and Christopher T. Sachrajda, “Pion Structure Functions From Lattice QCD,” *Phys. Lett. B* **196**, 184–190 (1987).
[13] C. Best, M. Göckeler, R. Horsley, Ernst-Michael Ilgenfritz, H. Perlt, Paul E. L. Rakow, A. Schäfer, G. Schierholz, A. Schiller, and S. Schramm, “Pion and rho structure functions from lattice QCD,” *Phys. Rev. D* **56**, 2743–2754 (1997), [arXiv:hep-lat/9703014](#).
[14] M. Guagnelli, K. Jansen, F. Palombi, R. Petronzio, A. Shindler, and I. Wetzorke (Zeuthen-Rome (ZeRo)), “Non-perturbative pion matrix element of a twist-2 operator from the lattice,” *Eur. Phys. J. C* **40**, 69–80 (2005), [arXiv:hep-lat/0405027](#).
[15] S. Capitani, K. Jansen, M. Papinutto, A. Shindler, C. Urbach, and I. Wetzorke, “Parton distribution functions with twisted mass fermions,” *Phys. Lett. B* **639**, 520–526 (2006), [arXiv:hep-lat/0511013](#).
[16] A. Abdel-Rehim *et al.*, “Nucleon and pion structure with lattice QCD simulations at physical value of the pion mass,” *Phys. Rev. D* **92**, 114513 (2015), [Erratum: *Phys. Rev. D* **93**, 039904 (2016)], [arXiv:1507.04936 \[hep-lat\]](#).
[17] M. Oehm, C. Alexandrou, M. Constantinou, K. Jansen,

- G. Koutsou, B. Kostrzewa, F. Steffens, C. Urbach, and S. Zafeiropoulos, “ $\langle x \rangle$ and $\langle x^2 \rangle$ of the pion PDF from lattice QCD with $N_f = 2+1+1$ dynamical quark flavors,” *Phys. Rev. D* **99**, 014508 (2019), arXiv:1810.09743 [hep-lat].
- [18] Constantia Alexandrou, Simone Bacchio, Ian Cloet, Martha Constantinou, Kyriakos Hadjiyiannakou, Gianis Koutsou, and Colin Lauer (ETM), “Mellin moments $\langle x \rangle$ and $\langle x^2 \rangle$ for the pion and kaon from lattice QCD,” *Phys. Rev. D* **103**, 014508 (2021), arXiv:2010.03495 [hep-lat].
- [19] Constantia Alexandrou, Simone Bacchio, Ian Cloet, Martha Constantinou, Kyriakos Hadjiyiannakou, Gianis Koutsou, and Colin Lauer (ETM), “Pion and kaon $\langle x^3 \rangle$ from lattice QCD and PDF reconstruction from Mellin moments,” *Phys. Rev. D* **104**, 054504 (2021), arXiv:2104.02247 [hep-lat].
- [20] Marius Löffler, Daniel Jenkins, Rudolf Rödl, Andreas Schäfer, Lisa Walter, Philipp Wein, Simon Weishäupl, and Thomas Wurm (RQCD), “Mellin moments of spin dependent and independent PDFs of the ρ and π ,” (2021), arXiv:2108.07544 [hep-lat].
- [21] Harvey B. Meyer and John W. Negele, “Gluon contributions to the pion mass and light cone momentum fraction,” *Phys. Rev. D* **77**, 037501 (2008), arXiv:0707.3225 [hep-lat].
- [22] Xiangdong Ji, “Parton Physics on a Euclidean Lattice,” *Phys. Rev. Lett.* **110**, 262002 (2013), arXiv:1305.1539 [hep-ph].
- [23] Jian-Hui Zhang, Jiunn-Wei Chen, Luchang Jin, Huey-Wen Lin, Andreas Schäfer, and Yong Zhao, “First direct lattice-QCD calculation of the x -dependence of the pion parton distribution function,” *Phys. Rev. D* **100**, 034505 (2019), arXiv:1804.01483 [hep-lat].
- [24] Huey-Wen Lin, Jiunn-Wei Chen, Zhouyou Fan, Jian-Hui Zhang, and Rui Zhang, “Valence-Quark Distribution of the Kaon and Pion from Lattice QCD,” *Phys. Rev. D* **103**, 014516 (2021), arXiv:2003.14128 [hep-lat].
- [25] Xiang Gao, Luchang Jin, Christos Kallidonis, Nikhil Karthik, Swagato Mukherjee, Peter Petreczky, Charles Shugert, Sergey Syritsyn, and Yong Zhao, “Valence parton distribution of the pion from lattice QCD: Approaching the continuum limit,” *Phys. Rev. D* **102**, 094513 (2020), arXiv:2007.06590 [hep-lat].
- [26] A. V. Radyushkin, “Quasi-parton distribution functions, momentum distributions, and pseudo-parton distribution functions,” *Phys. Rev. D* **96**, 034025 (2017), arXiv:1705.01488 [hep-ph].
- [27] Bálint Joó, Joseph Karpie, Kostas Orginos, Anatoly V. Radyushkin, David G. Richards, Raza Sabbir Sufian, and Savvas Zafeiropoulos, “Pion valence structure from Ioffe-time parton pseudodistribution functions,” *Phys. Rev. D* **100**, 114512 (2019), arXiv:1909.08517 [hep-lat].
- [28] Yan-Qing Ma and Jian-Wei Qiu, “Exploring Partonic Structure of Hadrons Using ab initio Lattice QCD Calculations,” *Phys. Rev. Lett.* **120**, 022003 (2018), arXiv:1709.03018 [hep-ph].
- [29] Raza Sabbir Sufian, Joseph Karpie, Colin Egerer, Kostas Orginos, Jian-Wei Qiu, and David G. Richards, “Pion Valence Quark Distribution from Matrix Element Calculated in Lattice QCD,” *Phys. Rev. D* **99**, 074507 (2019), arXiv:1901.03921 [hep-lat].
- [30] Raza Sabbir Sufian, Colin Egerer, Joseph Karpie, Robert G. Edwards, Bálint Joó, Yan-Qing Ma, Kostas Orginos, Jian-Wei Qiu, and David G. Richards, “Pion Valence Quark Distribution from Current-Current Correlation in Lattice QCD,” *Phys. Rev. D* **102**, 054508 (2020), arXiv:2001.04960 [hep-lat].
- [31] Constantia Alexandrou *et al.*, “Simulating twisted mass fermions at physical light, strange and charm quark masses,” *Phys. Rev. D* **98**, 054518 (2018), arXiv:1807.00495 [hep-lat].
- [32] Roberto Frezzotti, Pietro Antonio Grassi, Stefan Sint, and Peter Weisz (Alpha), “Lattice QCD with a chirally twisted mass term,” *JHEP* **08**, 058 (2001), arXiv:hep-lat/0101001.
- [33] R. Frezzotti and G. C. Rossi, “Twisted mass lattice QCD with mass nondegenerate quarks,” *Nucl. Phys. B Proc. Suppl.* **128**, 193–202 (2004), arXiv:hep-lat/0311008.
- [34] Y. Iwasaki, “Renormalization Group Analysis of Lattice Theories and Improved Lattice Action: Two-Dimensional Nonlinear O(N) Sigma Model,” *Nucl. Phys. B* **258**, 141–156 (1985).
- [35] R. Frezzotti and G. C. Rossi, “Chirally improving Wilson fermions. 1. O(a) improvement,” *JHEP* **08**, 007 (2004), arXiv:hep-lat/0306014.
- [36] R. Frezzotti and G. C. Rossi, “Chirally improving Wilson fermions. II. Four-quark operators,” *JHEP* **10**, 070 (2004), arXiv:hep-lat/0407002.
- [37] C. Alexandrou *et al.*, “Quark masses using twisted mass fermion gauge ensembles,” (2021), arXiv:2104.13408 [hep-lat].
- [38] Arjun Singh Gambhir, Andreas Stathopoulos, and Kostas Orginos, “Deflation as a Method of Variance Reduction for Estimating the Trace of a Matrix Inverse,” *SIAM J. Sci. Comput.* **39**, A532–A558 (2017), arXiv:1603.05988 [hep-lat].
- [39] Andreas Stathopoulos, Jesse Laeuchli, and Kostas Orginos, “Hierarchical probing for estimating the trace of the matrix inverse on toroidal lattices,” (2013), arXiv:1302.4018 [hep-lat].
- [40] Karl Jansen and Chuan Liu, “Implementation of Symanzik’s improvement program for simulations of dynamical Wilson fermions in lattice QCD,” *Comput. Phys. Commun.* **99**, 221–234 (1997), arXiv:hep-lat/9603008.
- [41] Colin Morningstar and Mike J. Peardon, “Analytic smearing of SU(3) link variables in lattice QCD,” *Phys. Rev. D* **69**, 054501 (2004), arXiv:hep-lat/0311018.
- [42] Sz. Borsanyi *et al.*, “Leading hadronic contribution to the muon magnetic moment from lattice QCD,” *Nature* **593**, 51–55 (2021), arXiv:2002.12347 [hep-lat].
- [43] We thank the authors of Ref. [44] for communicating their results at 2 GeV in the $\overline{\text{MS}}$ scheme.
- [44] P. C. Barry, Chueng-Ryong Ji, N. Sato, and W. Melnitchouk, “Global QCD analysis of pion parton distributions with threshold resummation,” (2021), arXiv:2108.05822 [hep-ph].
- [45] Ivan Novikov *et al.*, “Parton Distribution Functions of the Charged Pion Within The xFitter Framework,” *Phys. Rev. D* **102**, 014040 (2020), arXiv:2002.02902 [hep-ph].
- [46] Xiang-Dong Ji, “A QCD analysis of the mass structure of the nucleon,” *Phys. Rev. Lett.* **74**, 1071–1074 (1995), arXiv:hep-ph/9410274.
- [47] Xiang-Dong Ji, “Breakup of hadron masses and energy-momentum tensor of QCD,” *Phys. Rev. D* **52**, 271–281 (1995), arXiv:hep-ph/9502213.
- [48] Cédric Lorcé, “On the hadron mass decomposition,” *Eur. Phys. J. C* **78**, 120 (2018), arXiv:1706.05853 [hep-ph].

- [49] Yoshitaka Hatta, Abha Rajan, and Kazuhiro Tanaka, “Quark and gluon contributions to the QCD trace anomaly,” *JHEP* **12**, 008 (2018), arXiv:1810.05116 [hep-ph].
- [50] Kazuhiro Tanaka, “Three-loop formula for quark and gluon contributions to the QCD trace anomaly,” *JHEP* **01**, 120 (2019), arXiv:1811.07879 [hep-ph].
- [51] Andreas Metz, Barbara Pasquini, and Simone Rodini, “Revisiting the proton mass decomposition,” *Phys. Rev. D* **102**, 114042 (2020), arXiv:2006.11171 [hep-ph].
- [52] Jülich Supercomputing Centre, “JUQUEEN: IBM Blue Gene/Q Supercomputer System at the Jülich Supercomputing Centre,” *Journal of large-scale research facilities* **1** (2015), 10.17815/jlsrf-1-18.
- [53] Jülich Supercomputing Centre, “JURECA: Modular supercomputer at Jülich Supercomputing Centre,” *Journal of large-scale research facilities* **4** (2018), 10.17815/jlsrf-4-121-1.
- [54] Jülich Supercomputing Centre, “JUWELS: Modular Tier-0/1 Supercomputer at the Jülich Supercomputing Centre,” *Journal of large-scale research facilities* **5** (2019), 10.17815/jlsrf-5-171.
- [55] K. Jansen and C. Urbach, “tmLQCD: A Program suite to simulate Wilson Twisted mass Lattice QCD,” *Comput. Phys. Commun.* **180**, 2717–2738 (2009), arXiv:0905.3331 [hep-lat].
- [56] Abdou Abdel-Rehim, Florian Burger, Albert Deuzeman, Karl Jansen, Bartosz Kostrzewa, Luigi Scorzato, and Carsten Urbach, “Recent developments in the tmLQCD software suite,” *PoS LATTICE2013*, 414 (2014), arXiv:1311.5495 [hep-lat].
- [57] A. Deuzeman, K. Jansen, B. Kostrzewa, and C. Urbach, “Experiences with OpenMP in tmLQCD,” *PoS LATTICE2013*, 416 (2013), arXiv:1311.4521 [hep-lat].
- [58] Albert Deuzeman, Siebren Reker, and Carsten Urbach (ETM), “Lemon: an MPI parallel I/O library for data encapsulation using LIME,” *Comput. Phys. Commun.* **183**, 1321–1335 (2012), arXiv:1106.4177 [hep-lat].
- [59] M. A. Clark, R. Babich, K. Barros, R. C. Brower, and C. Rebbi, “Solving Lattice QCD systems of equations using mixed precision solvers on GPUs,” *Comput. Phys. Commun.* **181**, 1517–1528 (2010), arXiv:0911.3191 [hep-lat].
- [60] R. Babich, M. A. Clark, B. Joo, G. Shi, R. C. Brower, and S. Gottlieb, “Scaling Lattice QCD beyond 100 GPUs,” in *SC11 International Conference for High Performance Computing, Networking, Storage and Analysis Seattle, Washington, November 12-18, 2011* (2011) arXiv:1109.2935 [hep-lat].
- [61] M. A. Clark, Bálint Joó, Alexei Strelchenko, Michael Cheng, Arjun Gambhir, and Richard Brower, “Accelerating Lattice QCD Multigrid on GPUs Using Fine-Grained Parallelization,” (2016), arXiv:1612.07873 [hep-lat].
- [62] R Core Team, *R: A Language and Environment for Statistical Computing*, R Foundation for Statistical Computing, Vienna, Austria (2019).
- [63] Bartosz Kostrzewa, Johann Ostmeier, Martin Ueding, and Carsten Urbach, “hadron: package to extract hadronic quantities,” <https://github.com/HISKP-LQCD/hadron> (2020), R package version 3.0.1.

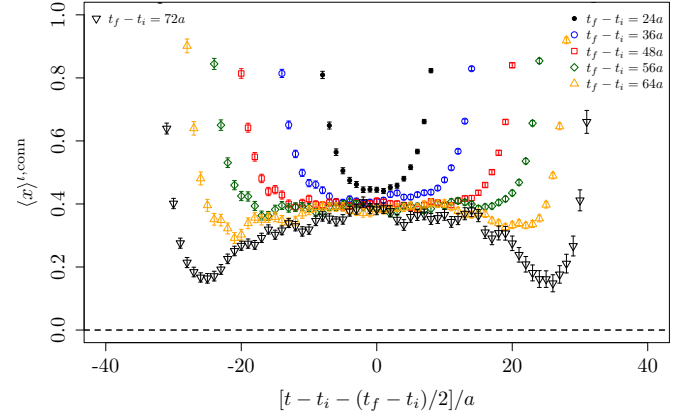


FIG. 4. Connected contribution to the bare $\langle x \rangle^l$ is shown for different values of $t_f - t_i$.

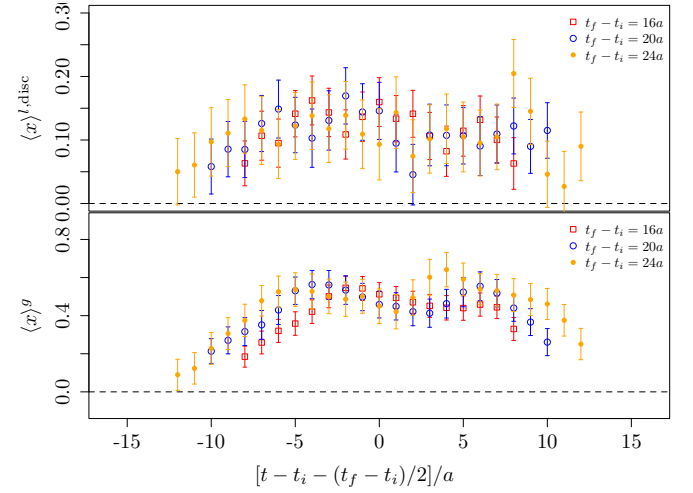


FIG. 5. Bare $\langle x \rangle^X$ as a function of $t - t_i$ for $X = l$ (disconnected only) and $X = g$. Different values of $t_f - t_i$ are shown and we only show $t \in [0, t_f - t_i]$.

APPENDIX

In this section we provide additional details on the analysis and additional figures. In Fig. 4 we show $\langle x \rangle^{l, \text{conn}}(t - t_i)$ for different source sink separations $t_f - t_i$. It is clearly observable that the plateau around $t - t_i - (t_f - t_i)/2 = 0$ becomes longer as $t_f - t_i$ increases. However, once $t_f - t_i > T/2$, deviations become larger again.

For the disconnected contributions we show as examples $\langle x \rangle^g(t - t_i)$ and $\langle x \rangle^{l, \text{disc}}$ in Fig. 5. It can be seen that the plateau region around $t - t_i - (t_f - t_i)/2 = 0$ is rather independent of the shown $t_f - t_i$ values, apart from increasing statistical uncertainties with increasing $t_f - t_i$ values. For $t_f - t_i = 32$ (not shown) errors are so large, that all points are compatible with zero for the fermionic disconnected contributions.

In Table II we give the bare values for all the contribu-

tions to $\langle x \rangle$.

Contribution	Operator	
$\langle x \rangle_l^{\text{conn}}$	\bar{T}_{44}	0.387(7)
$\langle x \rangle_l^{\text{disc}}$	\bar{T}_{4k}	0.116(23)
$\langle x \rangle_s$	\bar{T}_{4k}	0.0416(108)
$\langle x \rangle_c$	\bar{T}_{4k}	0.0074(43)
$\langle x \rangle_g$	\bar{T}_{4k}	0.498(61)

TABLE II. Bare values for the different contributions to $\langle x \rangle$.

Renormalisation

For convenience we reproduce here the renormalisation constants from Ref. [7]. The nonsinglet ones read

$$Z_{qq}^{\mu=\nu} = 1.151(1)(4), \quad Z_{qq}^{\mu \neq \nu} = 1.160(1)(3),$$

and the singlet ones

$$Z_{qq}^{s,\mu=\nu} = 1.161(18)(16), \quad Z_{qq}^{s,\mu \neq \nu} = 1.163(11)(5).$$

For the gluon

$$Z_{gg}^{\mu \neq \nu} = 1.08(17)(3),$$

all at 2 GeV in the $\overline{\text{MS}}$ scheme. The mixing coefficients Z_{gq} and Z_{qq} have been determined perturbatively in Ref. [7]. Their values read

$$\begin{aligned} Z_{gq}^{\mu=\nu} &= 0.232, & Z_{gq}^{\mu \neq \nu} &= 0.083, \\ Z_{qq}^{\mu=\nu} &= -0.027. \end{aligned} \quad (11)$$

Unfortunately, Z_{gq} is not available for $\mu \neq \nu$. However, since $Z_{gq}^{\mu \neq \nu} \ll Z_{gq}^{\mu=\nu}$ and $Z_{gq}^{\mu=\nu}$ itself is small compared to the other two, we assume here that $Z_{gq}^{\mu=\nu} = Z_{gq}^{\mu \neq \nu}$, also due to the fact that the divergent part in the two is identical.

Another question which needs to be discussed is the justification of treating connected and disconnected light contributions separately and even using different operators. It is based on the mixed action analysis performed by the authors of Ref. [36].

Consider the bare quark contribution to $\langle x \rangle$ for a twisted mass quark flavor χ not present in the simulated action with twisted quark mass μ_χ . The insertion \bar{T}^χ leads to a purely disconnected contribution. For such an insertion, at nonzero lattice spacing the corresponding $\langle x \rangle^\chi(\mu_\chi)$ is well defined from spectral decomposition. Lattice rotational symmetry instead guarantees *invariance* of $\langle x \rangle^\chi(\mu_\chi)$ w.r.t. the chosen tensor component *up to lattice artifacts*.

We use this *nonunitary* setup for the strange and charm quark contribution with any value of μ_s, μ_c . Note that lattice artefacts are then still of $\mathcal{O}(a^2)$ [36]. In the regularised theory the so obtained $\langle x \rangle^\chi(\mu_\chi)$ is a *smooth function* of the twisted valence quark mass μ_χ and we can have a well-defined limit to the unitary case

$$\lim_{\mu_\chi \rightarrow \mu_l} \langle x \rangle_{\mu_\chi}^\chi = \langle x \rangle^{l,\text{disc}}, \quad (12)$$

where results from different choices of tensor components only differ by lattice artefacts. Thus in the linear decomposition of $\langle x \rangle = \langle x \rangle^{l,\text{conn}} + \langle x \rangle^{l,\text{disc}}$ into a connected and disconnected contribution, the disconnected contribution $\langle x \rangle^{l,\text{disc}}$ is fixed up to lattice artefacts. Also the complete $\langle x \rangle^{l,\text{conn}} + \langle x \rangle^{l,\text{disc}}$ is invariant under change of tensor components by the remnant Lorentz symmetry.

In conclusion the employed decomposition into $\langle x \rangle^{l,\text{conn}} + \langle x \rangle^{l,\text{disc}}$ in the regularised theory is unique up to lattice artefacts. Moreover, the renormalisation pattern for diagonal and off-diagonal tensor elements is identical again up to lattice artefacts, which vanish in the continuum limit.

Note that the spectral decomposition of the relevant three-point function leads to a constant plus excited states. This is why there cannot be any delicate cancellation of exponential terms like in the case for instance of the η, η' correlation functions, where connected and disconnected contribution must not be analysed separately.

Quark mass tuning

The unitary light, strange and charm quark masses for the simulated lattice action are tuned such that the physical values of the pion mass, the ratio of charm and strange quark masses and the ratio of the D_s meson and its decay constant are reproduced as detailed in Ref. [31].

Within our mixed action setup, the bare mass of strange and charm quark, which enter the quark energy momentum tensor in our calculation, are tuned by matching the Ω^- and the Λ_c baryon mass to their physical values by the procedure in Ref. [37].

The numerical values of the bare strange and charm quark parameters read

$$a\mu_s = 0.0186, \quad a\mu_c = 0.2490. \quad (13)$$